



## The Condor seamount at Mid-Atlantic Ridge as a supplementary source of trace and rare earth elements to the sediments



Miguel Caetano<sup>a,\*</sup>, Carlos Vale<sup>a</sup>, Bárbara Anes<sup>a</sup>, Joana Raimundo<sup>a</sup>, Teresa Drago<sup>a</sup>, Sabine Schimdt<sup>b</sup>, Marta Nogueira<sup>a</sup>, Anabela Oliveira<sup>c</sup>, Ricardo Prego<sup>d</sup>

<sup>a</sup> IPMA—Portuguese Institute for Sea and Atmosphere, Av. Brasília, 1449-006 Lisboa, Portugal

<sup>b</sup> Bordeaux University—CNRS, Avenue de Facultés, 33405 Talence, France

<sup>c</sup> Instituto Hidrográfico, Rua das Trinas, 49, 1200 Lisbon, Portugal

<sup>d</sup> Marine Research Institute (CSIC), Av. Eduardo Cabello, 36208 Vigo, Spain

### ARTICLE INFO

Available online 16 January 2013

#### Keywords:

Condor seamount  
Sediments  
Rare earth elements  
Pb isotopes  
Metals  
Azores archipelago  
North Atlantic Ocean

### ABSTRACT

The Condor Seamount rises from seabed to 180 m water depth, being located 10 nautical miles southwest of the island of Faial, Azores Archipelago at the Mid-Atlantic Ridge (MAR). The vertical distribution of major, minor, trace and rare earth elements (REE) and Pb isotopes was studied in four sediment cores: one from the top of the Condor Seamount (200 m, MC9), two from the seamount base (1400 m, MC2 and MC4), and one from a deep area (1900 m, MC8). Sediments from the top of the Condor were composed by coarser particles being the fine fraction lower than 1%. Conversely the other sediments were constituted by 51–92% of fine particles (<63 μm). Individual fragments of volcanic material (>2 mm) were found at several depths of the cores sampled at the base of the seamount. The core collected in the top of the Condor showed higher carbonate content (76–86%) compared with the other cores (41–64%). The chemical compositions of MC2 and MC4 point to an enhancement of V, Cr, Co, Ni and Fe concentrations. Lower concentrations in MC8 hypothesis that Condor seamount constitutes a supplementary source of trace elements. The most plausible explanation for the enhancement found in sediments of the seamount base is the weathering of slopes with volcanic activities, which supply particles with higher element concentrations than pelagic sediments. This hypothesis is corroborated by REE data, showing increased chondrite normalized ratios in MC2 and MC4. Moreover, the REE pattern found in those cores was comparable to that existing in volcanic material with Light REE enrichment in comparison to Heavy REE. These results indicate a substantial contribution of particles derived from volcanic activities to sediments settled in the vicinity of the Condor Seamount. It is argued the potential use of REE in sediments from this region as tracers of volcanic activities. Depth profiles of <sup>206</sup>Pb/<sup>207</sup>Pb and <sup>206</sup>Pb/<sup>208</sup>Pb showed lower ratios in the first 8 cm sediment layers, reflecting atmospheric input of anthropogenic Pb in the last century. On the basis of Pb profiles it is proposed a baseline Pb concentration of  $3.6 \pm 0.2 \mu\text{g g}^{-1}$  for pelagic sediments of the region with an isotopic signature of <sup>206</sup>Pb/<sup>207</sup>Pb =  $1.227 \pm 0.003$  and <sup>206</sup>Pb/<sup>208</sup>Pb =  $0.492 \pm 0.001$  signature. The isotope plots of <sup>206</sup>Pb/<sup>207</sup>Pb versus <sup>208</sup>Pb/<sup>206</sup>Pb showed a linear trend indicating the mixing between more radiogenic pre-industrial end-members and less radiogenic anthropogenic lead. The Pb isotope composition of sediments from the Condor area falls closer to North Atlantic Sediment Line. Sediments showed a <sup>206</sup>Pb/<sup>204</sup>Pb signature closer to the basalts of the Capelo volcanic complex than from Mid-Ocean Ridge Basalts (MORB), which suggests the contribution of similar geological formations to sedimentary material.

© 2013 Elsevier Ltd. All rights reserved.

### 1. Introduction

The concentration of trace elements and rare earth elements (REE) in pelagic and oceanic sediments reflects the balance

between chemical, oceanographic and sedimentary controls on their supply to, distribution in and removal from the ocean (Calvert and Pedersen, 1993; Morford and Emerson, 1999). Post-depositional reactions in bottom sediments may lead to element recycling or deep burial (Berner, 1980). Ancient black shales often exhibit higher trace element concentrations than modern sediments resulting from the supply of hydrothermal or volcanic sources (Calvert and Pedersen, 1993). Several works have been

\* Corresponding author. Tel.: +351 213027073; fax: +351 213015947.  
E-mail address: [mcaetano@ipma.pt](mailto:mcaetano@ipma.pt) (M. Caetano).

developed in sedimentary environments close to active submarine hydrothermal sites either associated with Mid-Ocean Ridge (MOR) or associated with exposed serpentinized peridotites (e.g. Chavagnac et al., 2005; Dias et al., 2011; Dosso et al., 1999; Edmonds and German, 2004). These works have been focus on the understanding of hydrothermal processes using sediments, massive sulfides and altered rocks as a recorder of hydrothermal activity. Furthermore, hydrothermal sediments have a distinct mineralogical and geochemical signature in comparison to normal pelagic sediments (Boström and Peterson, 1969; Mills and Elderfield, 1995). The deposition of volcanoclastic debris, namely volcanic glass and plagioclase in pelagic sediments is usually found in areas closer to sites with submarine or terrestrial volcanism (Berner, 1980; Zhou et al., 2000). The deposition of a single layer of ashes may create a record of the volcanic event although bioturbation and biodiffusion processes may smear the initial signal (Burdige, 2006). Post-depositional mixing or mixing of material produced from different eruptions with pelagic sediment tends to create thus compositionally heterogeneous sedimentary material enhancing the problem of vertical identification of the volcanic episodes (Mascarenhas-Pereira et al., 2006). Nevertheless, if trace elements and REE concentrations in ashes remain relatively immobile during the processes of surface alteration and diagenesis (Zhou et al., 2000) zones directly influenced by volcanic activities may be identified. Rare earth elements have the particularity of being less susceptible to mutual fractionation in geochemical processes and simplifying the interpretation of these spatial patterns (Santos et al., 2007). The proportion of Light REE relative to Middle REE or Heavy REE, as well as Ce and Eu anomalies, have been widely used to characterize rocks, sediments or fluids from different hydrothermal origins (e.g. Chavagnac et al., 2005; Dias and Barriga, 2006; Dias et al., 2011; Douville et al., 2002).

Stable Pb isotope ratios exhibit spatial variability in the sea, reflecting differences in the sources of oceanic Pb (Gobeil et al., 2001; Muiños et al., 2008; Véron et al., 1994), ocean circulation and ultimate removal of Pb (e.g. Alleman et al., 1999; Henderson

and Maier-Reimer, 2002; Véron et al., 1999). Lead isotopes could, therefore, provide information about the past distribution of continental weathering fluxes to the ocean (Henderson and Maier-Reimer, 2002). Lead isotopes display more radiogenic signatures in ocean islands, as well as broad intervals, than in Mid Oceanic Ridge Basalts (MORB) due to plume source heterogeneities, material entrainment during plume ascent or interaction between plumes and the lithosphere (Moreira et al., 1999). The supply of this material to pelagic sediments may also introduced changes in their Pb signature during time.

Seamounts are among the most common topographic features in the world ocean (Wessel et al., 2010). The occurrence of seamounts in the North Atlantic is often imputable to the volcanic and tectonically active seafloor along the Mid-Atlantic Ridge (MAR). Condor is a ridge seamount located about 10 nm to the WSW of Faial Island in the Azores Archipelago (Fig. 1). The seamount is an elongated ridge with a WNW–ESE orientation being the major semi-axis of 35 km. Its outer edge, delineated using the farthest convex bathymetric contours that radiated from the main ridge, is roughly outlined by the 1700-m depth contour along the edge farthest from Faial Island (Tempera et al., 2012). Its orientation is parallel with the main volcanic ridges in the area south of the Terceira rift, including the Faial–Pico complex (Lourenço et al., 1998). The morphology resulted most likely from the accumulation of lavas produced by multiple superimposed cones or ridges that erupted from volcanic dykes oriented along its main axis. The seamount has a flat summit area suggesting that surface was previously at this level during periods of lowered sea level. Because the shallowest point of the seamount at 184 m depth is below maximum depth of sea-level lowstands commonly considered to have occurred during the Pleistocene (Vogt and Jung, 2004). The water column above the summit is characterized by a checkered pattern of temperature and salinity fields consisting of two upwelling centers (with higher turbidity levels) entwined with two downwelling centers. The mixed layer may extend down to 200 m depth during the cold season, therefore intersecting the seamount summit and possibly influencing its biological assemblages (Tempera et al., 2012).

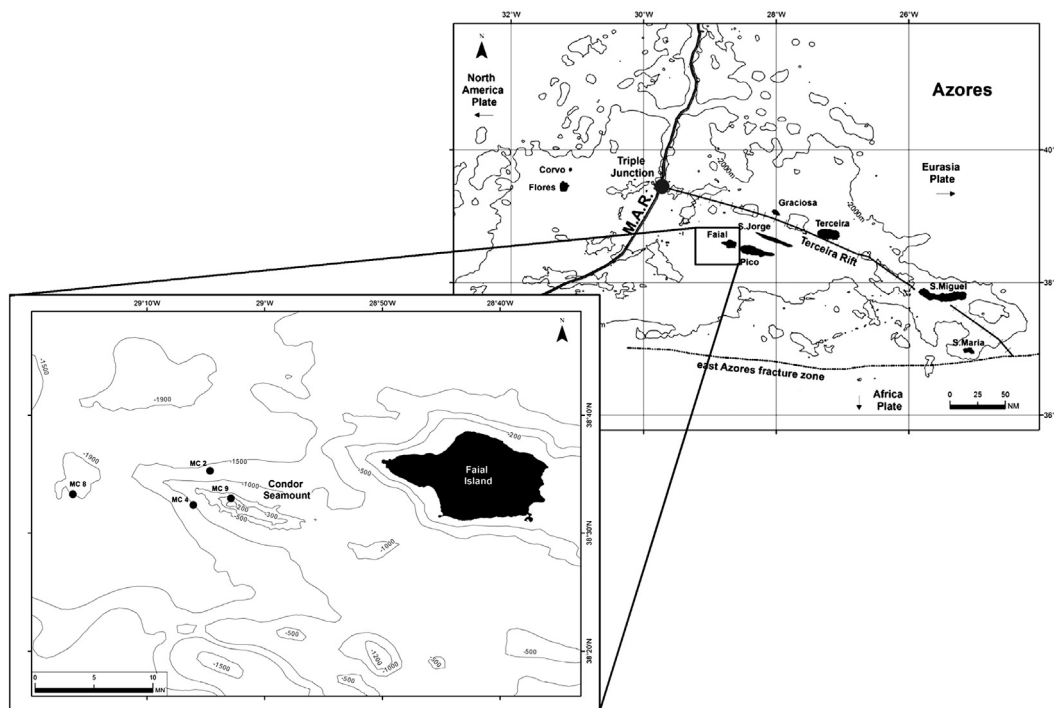


Fig. 1. Location of the Condor seamount and the sampled cores.

Several works on trace element geochemistry have been published in the Mid-Atlantic Ridge (MAR) closer to hydrothermal vents (Cave et al., 2002; Chavagnac et al., 2005; Dias and Barriga, 2006; Dias et al., 2008, 2010, 2011; Dosso et al., 1999; Hamelin et al., 1984; López-García et al., 2003; Marques et al., 2007). Despite the relevance of the Condor seamount as habitat, to fisheries in a peculiar situation being close to islands with recent episodes of volcanism in sea, geochemistry of the area is poorly documented. In fact, shallow hydrothermal vents were recently discovered closer to the Faial Island (Giovannelli et al., 2012). The extent and the impact of fluids from these vents in the adjacent non-hydrothermal ecosystems such as the seamounts are unknown. This work reports grain size, carbonate, organic carbon contents, mineralogical compositions, major, trace and rare earth element concentrations, values of excess  $^{210}\text{Pb}$  and stable Pb isotopic ratios in four short sediment cores collected in the top of the Condor seamount, in its base and in a deep area nearby. Differences on sediment composition among sites and with depth are interpreted taking into consideration the specificity of the region. Additionally REE distribution is also tested as a proxy of volcanic activity.

## 2. Material and methods

### 2.1. Sampling

Four short-sediment cores were sampled onboard of the R.V. Noruega, using a Multi-corer MARK II—400 in July 2010 at the Condor seamount and vicinity area (Fig. 1): MC9 (38°32.94'N; 29°02.87'W, 200 m water depth) in the top of the seamount; MC2 (38°35.26'N; 29°04.65'W, 1290 m) and MC4 (38°32.38'N; 29°06.07'W, 1006 m) in the base of the seamount; and MC8 (38°33.3'N; 29°16.3'W, 1900 m) in a deeper zone located 10 nm west from the seamount. The length of the cores were: 11 cm (MC9), 14 cm (MC4 and MC8) and 32 cm (MC2). Cores were sliced immediately after sampling in 1-cm thickness layers until 10 cm depth and in 2-cm for deeper layers.

Volcanic fragments (larger than 2 mm) found in MC2 (3–4 cm and 6–7 cm) and MC4 (4–5 cm, 5–6 cm and 8–9 cm) were separated from the bulk sediment and washed for chemical analysis. Washing may not have removed particles incrustated in the sampled fragments. A composite basalt sample was also collected from the Capelo volcanic complex in the Faial Island. Sediment and fragment samples were oven dried at 40 °C pending for sedimentological and geochemical analysis.

### 2.2. Analytical methods

#### 2.2.1. Grain-size and carbonates

Analysis of grain-size distribution was performed on 5–10 g of sediment by means of the traditional sieving method (Retsch AS-200) and sediments were classified according to Flemming (2000). Carbonate content was determined following the Eijkelkamp volumetric methodology that meets the standard ISO 10693.

#### 2.2.2. Mineralogy

The mineralogy was determined in sands of MC2 and MC8 by the stereomicroscope observation following the procedure described in Dias (1987). Fine fraction mineralogy was carried out in the same cores using X-Ray Diffraction (XRD) following Oliveira et al. (2007). The two cores were selected due to their proximity to the volcanic Capelo complex (Fig. 1).

#### 2.2.3. Carbon

Carbon sediment content was measured in homogenized and dried sediments, using a CHN Fisons NA 1500 Analyzer. Procedural blanks were obtained by running several empty ash tin capsules.

Organic carbon was estimated by finding the difference between total carbon and inorganic carbon after heating samples at 450 °C for 2 h in order to remove the organic carbon from the sediment.

#### 2.2.4. Lead-210

The  $^{210}\text{Pb}$  radiochronology was performed in cores MC2 and MC8 since those represent the closer and far away environments, respectively, from Condor seamount and volcanic Capelo complex. Radionuclide measurements were made over 9 levels in MC2 and 7 levels in MC8 on dry homogenized samples using a semi-planar germanium detector (EGSP 2200-25-R from EURYSIS Mesures) (Schmidt et al., 2007). The activities of  $^{210}\text{Pb}$  and  $^{137}\text{Cs}$  were determined by direct measurement of their gamma decay energy at 46.5 and 661.7 keV respectively;  $^{226}\text{Ra}$  through its daughter products  $^{214}\text{Pb}$  (295.2 keV and 352.0 keV) and  $^{214}\text{Bi}$  (609.3 keV). Error on radionuclide activities are based on 1 standard deviation counting statistics. Excess  $^{210}\text{Pb}$  activities were calculated by subtracting the activity supported by its parent isotope,  $^{226}\text{Ra}$ , from the total activity in the sediment. Errors on  $^{210}\text{Pb}_{\text{xs}}$  are calculated by propagation of errors in  $^{210}\text{Pb}$  and  $^{226}\text{Ra}$ . Sediment accumulation rate can be derived from  $^{210}\text{Pb}$ , based on two assumptions: constant flux and constant sediment accumulation rates (referred to as the CF:CS method) (Robbins and Edgington, 1975). Sedimentation rates were calculated without considering bioturbation effects, representing maxima values.

#### 2.2.5. Elemental composition

Approximately 100 mg of sediments (fraction < 2 mm), volcanic fragments and basalt samples were grounded with an agate mortar and completely digested with 6 cm<sup>3</sup> of HF (40%) and 1 cm<sup>3</sup> of Aqua Regia (HCl-36%: HNO<sub>3</sub>-60%; 3:1) in closed Teflon bombs at 100 °C for 1 h (Rantala and Loring, 1975). The contents of the bombs were poured into 100 cm<sup>3</sup> volumetric flasks containing 5.6 g H<sub>3</sub>BO<sub>3</sub> and filled up with ultrapure Milli-Q water (18.2 MΩ cm). Major and minor elements were analyzed by flame atomic absorption spectrometry (Perkin Elmer AA100) with a nitrous oxide-acetylene flame (Al, Si, Ca and Mg) and an air-acetylene flame (Fe and Mn). Elemental concentrations were determined with the standard addition method. For the analysis of trace elements, stable Pb isotopes and rare earth elements ground samples (≈ 100 mg) were digested using HF-HNO<sub>3</sub>-HCl in the proportions indicated above and the residue obtained was evaporated to near dryness in Teflon vials (DigiPrep HotBlock—SCP Science), redissolved with 1 cm<sup>3</sup> of double-distilled HNO<sub>3</sub> and 5 cm<sup>3</sup> of Milli-Q water, heated for 20 min at 75 °C, added 25 cm<sup>3</sup> of Milli-Q water, heated for 20 min at 90 °C and diluted to 50 cm<sup>3</sup> with Milli-Q water (Caetano et al., 2007, 2009; Hu and Gao, 2008). Trace elements, REE and stable Pb isotopes were determined in the same samples but in separate runs using a quadrupole ICP-MS (Thermo Elemental, X-Series) equipped with a Peltier Impact bead spray chamber and a concentric Meinhard nebulizer. The experimental parameters for trace elements and REE are detailed in Caetano et al. (2009). Three procedural blanks were prepared using the analytical procedures and reagents, and included in each batch of 20 samples.  $^{115}\text{In}$  was the internal standard chosen. The isotopes selected for the quantification of trace elements and REE were either free from, or subject to minimum isobaric and polyatomic interferences (Caetano et al., 2009; Smirnova et al., 2003). Quality control (QC) solutions for trace elements and REE were run every 10 samples. For all the elements analyzed, coefficients of variation for counts ( $n=5$ ) were lower than 2% and a 10-point calibration within a range of 1 to 200 μg L<sup>-1</sup> was used for quantification. Procedural blanks always accounted for less than 1% of element concentrations in the samples. The precision and accuracy of the analytical procedures was controlled through repeated analysis of the elements studied in certified reference

**Table 1a**  
 Certified and measured average concentrations and standard deviations of Al, Si, Ca, Mg, Fe (%), Mn, V, Cr, Co, Ni, Cu, As, Cd and Pb ( $\mu\text{g g}^{-1}$ ) in the certified reference materials from National Research Council of Canada.

CRM	Al	Si	Ca (%)	Mg	Fe	Mn	V	Cr	Co	Ni ( $\mu\text{g g}^{-1}$ )	Cu	As	Cd	Pb
MESS-2														
Certified	8.6 ± 0.3	-	-	-	4.35 ± 0.22	365 ± 21	252 ± 10	106 ± 8	13.8 ± 1.4	49.3 ± 1.8	39.3 ± 2	20.7 ± 0.8	0.24 ± 0.01	21.9 ± 1.2
Measured	8.8 ± 0.1	-	-	-	4.50 ± 0.22	357 ± 5	245 ± 7	110 ± 6	14.0 ± 0.6	48.0 ± 5.3	40 ± 3.9	21.0 ± 2.5	0.23 ± 0.04	22.0 ± 2.6
PACS-2														
Certified	6.62 ± 0.32	28 <sup>a</sup>	1.96 ± 0.18	1.47 ± 0.13	4.09 ± 0.06	440 ± 19	133 ± 5	90.7 ± 4.6	11.5 ± 0.3	39.5 ± 2.3	310 ± 12	26.2 ± 1.5	2.11 ± 0.15	183 ± 8
Measured	6.60 ± 0.20	27 ± 3	1.90 ± 0.61	1.50 ± 0.20	4.00 ± 0.05	426 ± 9	132 ± 4	91.0 ± 0.8	11.0 ± 0.9	39.2 ± 0.4	311 ± 4	25.8 ± 0.3	2.06 ± 0.03	186 ± 2

<sup>a</sup> Informative values.

**Table 1b**  
 Certified and measured average concentrations of rare earth elements (La, Ce, Pr, Nd, Sm, Eu, Gd, Tb, Dy, Ho, Er, Tm, Yb and Lu) in  $\mu\text{g g}^{-1}$  and standard deviations in the certified reference materials AGV-1 from United States Geological Survey.

CRM	La	Ce	Pr	Nd	Sm	Eu	Gd	Tb ( $\mu\text{g g}^{-1}$ )	Dy	Ho	Er	Tm	Yb	Lu
AGV-1														
Certified	41 ± 2	67 ± 6	9.11 ± 0.05	33 ± 3	5.9 ± 0.4	1.6 ± 0.1	5.0 ± 0.6	0.7 ± 0.1	3.6 ± 0.4	0.72 ± 0.14	1.88 ± 0.04	0.27 ± 0.01	1.72 ± 0.20	0.25 ± 0.03
Measured	45 ± 4	63 ± 2	8.50 ± 0.50	32.4 ± 0.8	5.70 ± 0.04	1.7 ± 0.1	5.4 ± 0.1	0.7 ± 0.1	3.5 ± 0.1	0.68 ± 0.01	1.88 ± 0.04	0.26 ± 0.01	1.69 ± 0.04	0.25 ± 0.10

materials (MESS-2 and PACS-2 from the National Research Council of Canada and AGV-1 from the United States Geological Survey) (Tables 1a and 1b). Recoveries of analyzed elements were consistent with certified values in the reference standards.

### 2.2.6. Stable lead isotopes

The experimental conditions to measure the stable Pb isotopes ( $^{204}\text{Pb}$ ,  $^{206}\text{Pb}$ ,  $^{207}\text{Pb}$  and  $^{208}\text{Pb}$ ) described in Caetano et al. (2007). Between every two samples, corrections for mass fractionation

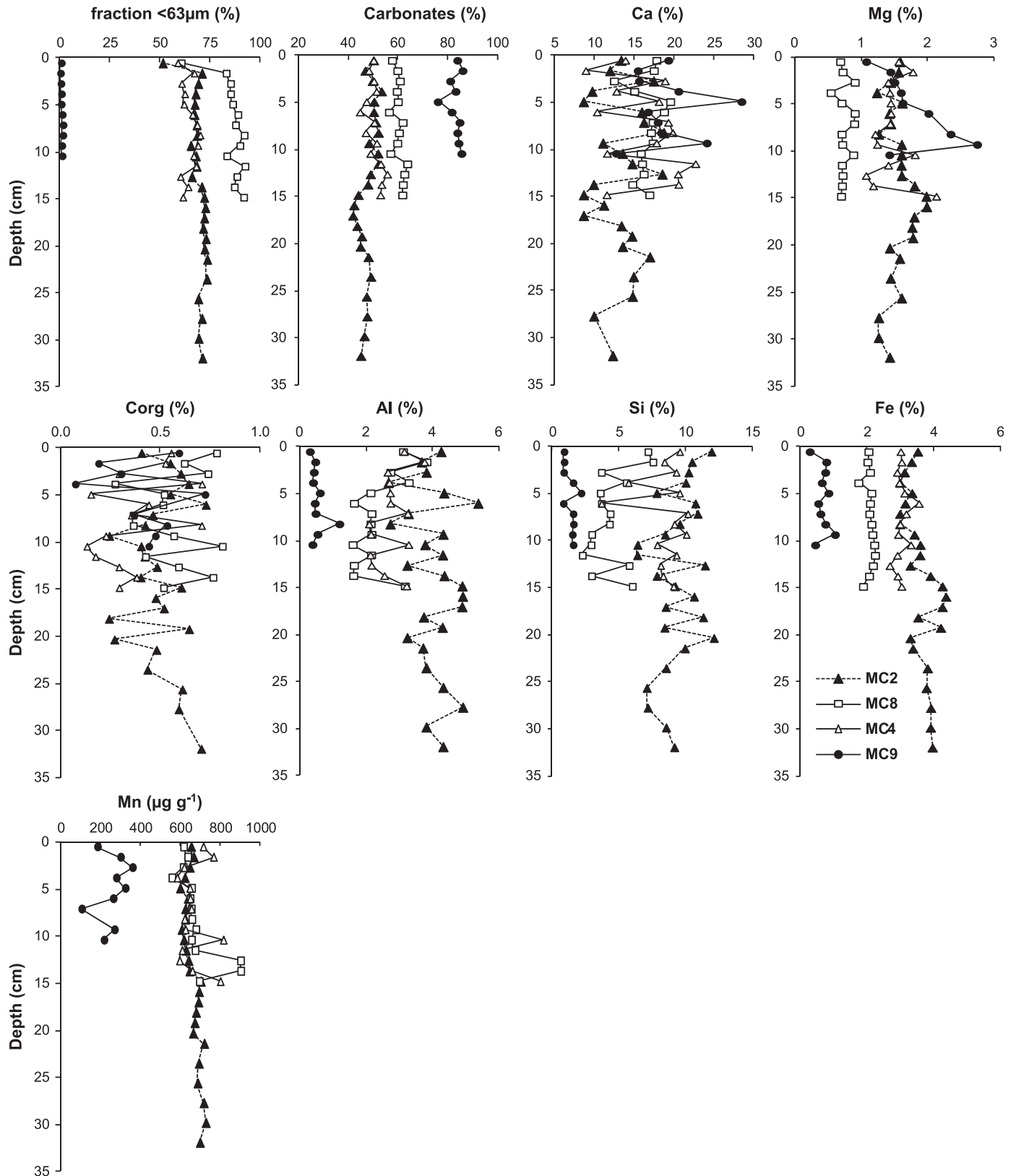


Fig. 2. Depth variation of Al, Si, Ca, Mg, Fe (%), Mn ( $\mu\text{g g}^{-1}$ ) and  $C_{\text{inorg}}$  (%) levels in the two cores collected in the Condor base (MC2 and MC4), one in the top of the seamount (MC9) and other far from it (MC8).

were applied using NIST SRM 981 (National Institute of Standard and Technology—Common Lead Isotopic Standard Material) reference material. No isobaric interference corrections are required for  $^{206}\text{Pb}$ ,  $^{207}\text{Pb}$  and  $^{208}\text{Pb}$  analysis, whereas  $^{204}\text{Pb}$  measurements require  $^{204}\text{Hg}$  correction via  $^{202}\text{Hg}$  (Reuer et al., 2003). The Pb isotopic composition of procedural blanks did not influence significantly the  $^{206}\text{Pb}/^{207}\text{Pb}$ ,  $^{206}\text{Pb}/^{204}\text{Pb}$ ,  $^{208}\text{Pb}/^{204}\text{Pb}$  and  $^{206}\text{Pb}/^{208}\text{Pb}$  ratios measured in sediment samples. The coefficients of variation of the NIST SRM 981 reference material obtained in between-batch external quality control were 0.37% for  $^{206}\text{Pb}/^{207}\text{Pb}$  and 0.22% for  $^{206}\text{Pb}/^{208}\text{Pb}$  ratios.

### 3. Results

#### 3.1. Major constituents

Vertical profiles of the major constituents of sediments from MC2, MC4, MC8 and MC9 are shown in Fig. 2. The whole chemical composition dataset is given in Electronic supplementary material. Sediments of MC8, MC2 and MC4 were composed of 60–92%, 51–73% and 59–70% of fine particles ( $< 63\ \mu\text{m}$ ), being classified as sandy-mud according to Flemming (2000). Sediments

of MC9 consisted of coarser particles with a fine fraction below 1%. Individual volcanic fragments larger than 2 mm were found in the top 10-cm sediment layer of cores MC2 and MC4. Minor fragments included in the sand fraction (63–2000  $\mu\text{m}$ ) were found in all sediment layers of these two cores. The volcanic basalt particles were more abundant in MC2, being found 5–17% of plagioclase (anorthite) and  $< 7\%$  of pyroxene (diopside), while in MC8 the plagioclase was vestigial ( $< 4\%$ ) and pyroxene absent. The sand fraction of MC2 and MC4 contained mainly planktonic foraminifera (68–70%). The fine fraction consisted mainly of biogenic calcite forms ( $> 72\%$ ) while aragonite and anorthite were present as minor constituents. Shell fragments and other biogenic debris were observed in MC9.

Carbonate content varied from 42% in MC2 to 86% in MC9 (top of the Condor). Calcium concentrations varied irregularly with the depth in all cores (8.7–28%) although values above 20% were only found in MC9. Magnesium were also presented at higher values in MC9 (1.0–2.9%) than in MC2 and MC4 (1.2–2.0%) and MC8 (0.5–0.9%). Organic carbon content varied irregularly with depth in all cores and was always lower than 0.7%. Concentrations of Al, Si and Fe were much lower in MC9 (0.2–1.2%, 1.1–2.1% and 0.1–1.1%) than in MC2 and MC4 (2.1–5.4%, 5.7–12% and 2.7–4.4%). An intermediate situation was found for the core MC8

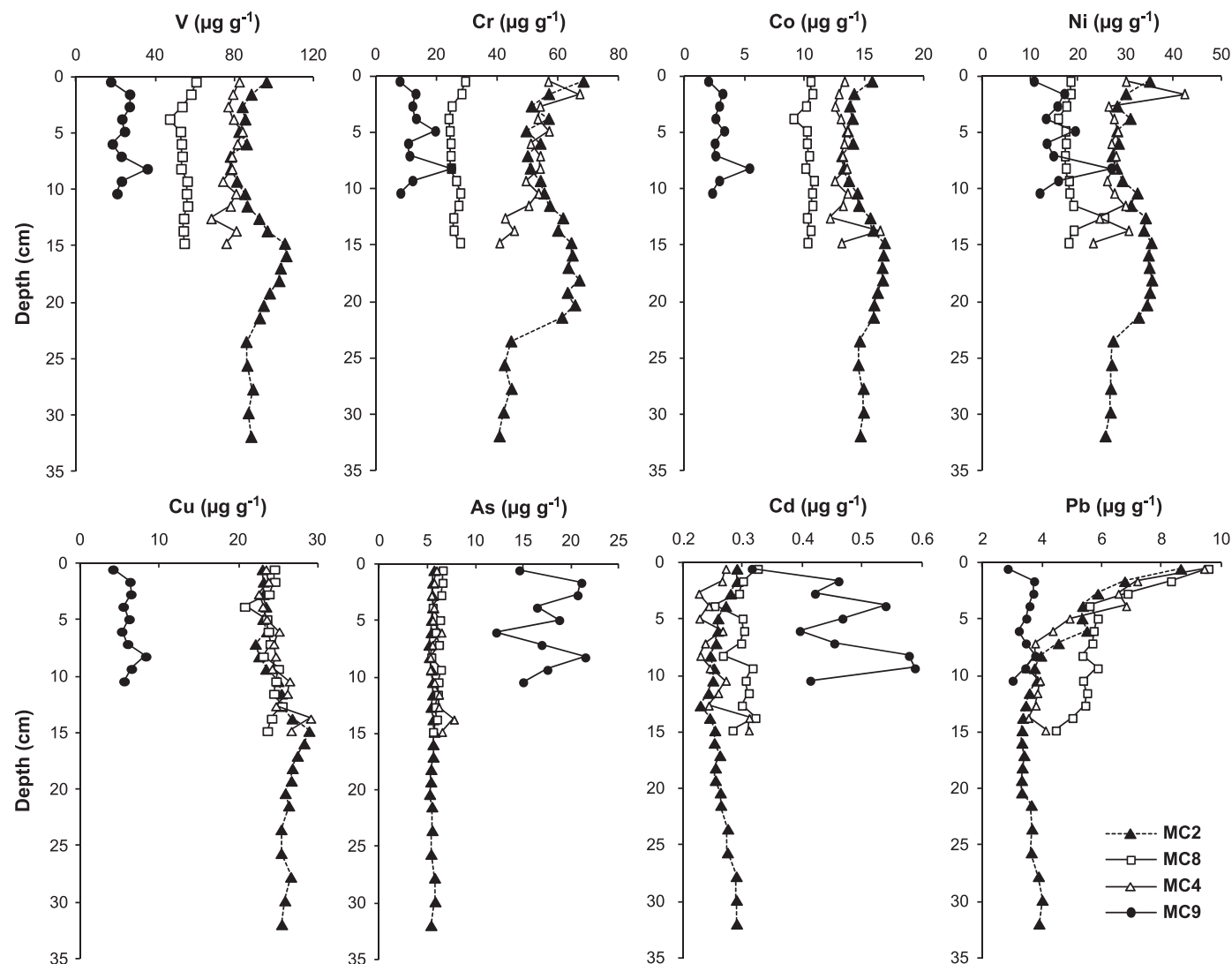


Fig. 3. Depth variation of V, Cr, Co, Ni, Cu, As, Cd and Pb ( $\mu\text{g g}^{-1}$ ) concentrations in the two cores collected in the Condor base (MC2 and MC4), one in the top of the seamount (MC9) and other far from it (MC8).

(Al=1.6–3.8%, Si=2.2–7.5% and Fe=1.8–2.3%). The depth profile of Fe concentrations showed a different pattern from the other elements with several subsurface broad enrichments. Manganese concentration was much lower in MC9 (105–359  $\mu\text{g g}^{-1}$ ) than in MC2, MC8 and MC4 (556–900  $\mu\text{g g}^{-1}$ ). Unlike other cores, MC8 showed a maximum of Mn concentration between 12 and 14 cm depth. No significant correlations ( $p > 0.05$ ) between concentrations of major constituents were obtained.

### 3.2. Trace elements

Depth profiles of V, Cr, Co, Ni, Cu, As, Cd and Pb concentrations in cores MC9, MC2, MC4 and MC8 are represented in Fig. 3 and as Electronic supplementary material. Four distribution patterns can be discerned. Firstly, V, Cr, Co and Ni concentrations were higher in MC2 and MC4 (base of the seamount) than in MC8 and in MC9. Vertical profiles of these elements showed slight increased concentrations in the top sediments of MC2, MC4 and MC8. The differences of V, Cr and Co concentrations among cores (3–5 fold) were comparable to those observed for Fe, being found strong correlations between these elements: V–Fe ( $r=0.977$ ,  $p < 0.01$ ), Cr–Fe ( $r=0.891$ ,  $p < 0.01$ ), Co–Fe ( $r=0.962$ ,  $p < 0.01$ ). Secondly, Cu levels were comparable in MC2, MC4 and MC8 (21–29  $\mu\text{g g}^{-1}$ ) and were one order of magnitude above the values in MC9 (4.1–8.3  $\mu\text{g g}^{-1}$ ). The magnitude of those differences is comparable to the one observed for Mn, although no correlation was found between these two elements. The third pattern was defined by As and Cd. Otherwise other elements, the concentration ranges in MC9 (11–21  $\mu\text{g g}^{-1}$  for As and 0.32–0.59  $\mu\text{g g}^{-1}$  for Cd) were above those found in MC2, MC4 and MC8 (5.1–7.7  $\mu\text{g g}^{-1}$  for As and 0.23–0.33  $\mu\text{g g}^{-1}$  for Cd). Lead concentrations in MC9 were uniform with the depth, while in MC2, MC4 and MC8 it was registered an accentuated decrease with the depth. The decrease in the upper 8 cm of MC2 and MC4 was almost linear, varying from 9–10  $\mu\text{g g}^{-1}$  to 3.5  $\mu\text{g g}^{-1}$ .

### 3.3. Lead-210 activities

The depth variation of excess  $^{210}\text{Pb}$  in MC2 and MC8 is characterized by an exponential decrease down to 6 cm depth (Fig. 4). There was a slight increase of activities at 8 and 12 cm depth in MC8 presumably related to changes in sedimentation rates or non-local mixing of  $^{210}\text{Pb}_{\text{xs}}$ -enriched surface sediment. These observations and the presence of worm tubes point to non-diffusive bioturbation of the surface sediment as reported by Boudreau (1986). Activities of  $^{210}\text{Pb}_{\text{xs}}$  reached negligible levels ( $< 5 \text{ mBq g}^{-1}$ ) at 8 cm in MC2 and at 14 cm in MC8. Activities of  $^{137}\text{Cs}$  (not shown) were only observed in the uppermost sediment layers ( $< 3 \text{ mBq g}^{-1}$ ). As for  $^{210}\text{Pb}$  excess,  $^{137}\text{Cs}$  presented a slightly deeper penetration in MC8 (4–5 cm) than in MC2 (3–4 cm). Assuming constant flux of particles to the sediment surface, the  $^{210}\text{Pb}$  excess allows estimating the maximum sedimentation rates: 0.063  $\text{cm yr}^{-1}$  for MC2 and 0.059  $\text{cm yr}^{-1}$  for MC8. Values from these estimations agree with the deepest penetration of  $^{137}\text{Cs}$ .

### 3.4. Signature of stable Pb isotopes

The  $^{206}\text{Pb}/^{207}\text{Pb}$ ,  $^{206}\text{Pb}/^{208}\text{Pb}$  and  $^{206}\text{Pb}/^{204}\text{Pb}$  ratios in four collected cores are presented in Fig. 5a (MC2 and MC8) and Fig. 5b (MC4 and MC9). Isotopic composition of all sediment layers is also given in Electronic supplementary material. Although with some scattering variation a general gradual decrease of these ratios from 7-cm depth towards the sediment surface was found for MC2, MC4 and MC8. Topmost sediment layer of the four cores showed comparable Pb isotopic ratios

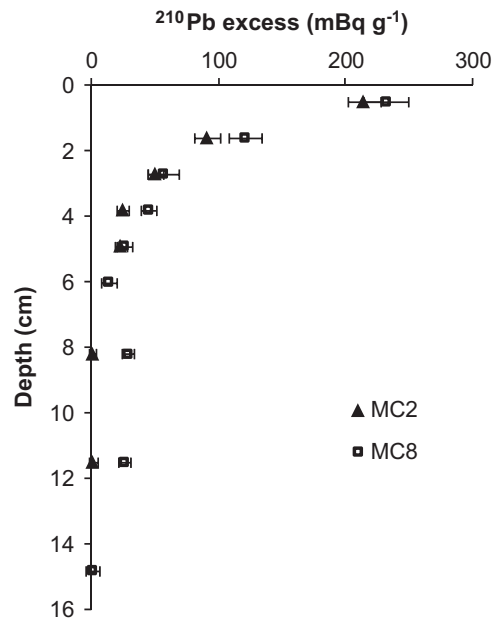


Fig. 4. Vertical profile of excess  $^{210}\text{Pb}$  in cores MC2 and MC8. Error bars represent standard deviations.

(e.g.  $^{206}\text{Pb}/^{207}\text{Pb}$  for MC2=1.199  $\pm$  0.001, MC4=1.207  $\pm$  0.002, MC8=1.198  $\pm$  0.001, MC9=1.196  $\pm$  0.001). An overlap of depth profiles was registered in the top 7-cm sediment layer of MC2 and MC8. Below 13 cm high radiogenic values were found in MC2 and MC4, but not observed at 15 cm depth in MC8. Less radiogenic values were found along the 11 cm of the core MC9 ( $^{206}\text{Pb}/^{207}\text{Pb}$ =1.198  $\pm$  0.002,  $^{206}\text{Pb}/^{208}\text{Pb}$ =0.486  $\pm$  0.001,  $^{206}\text{Pb}/^{204}\text{Pb}$ =18.73  $\pm$  0.07).

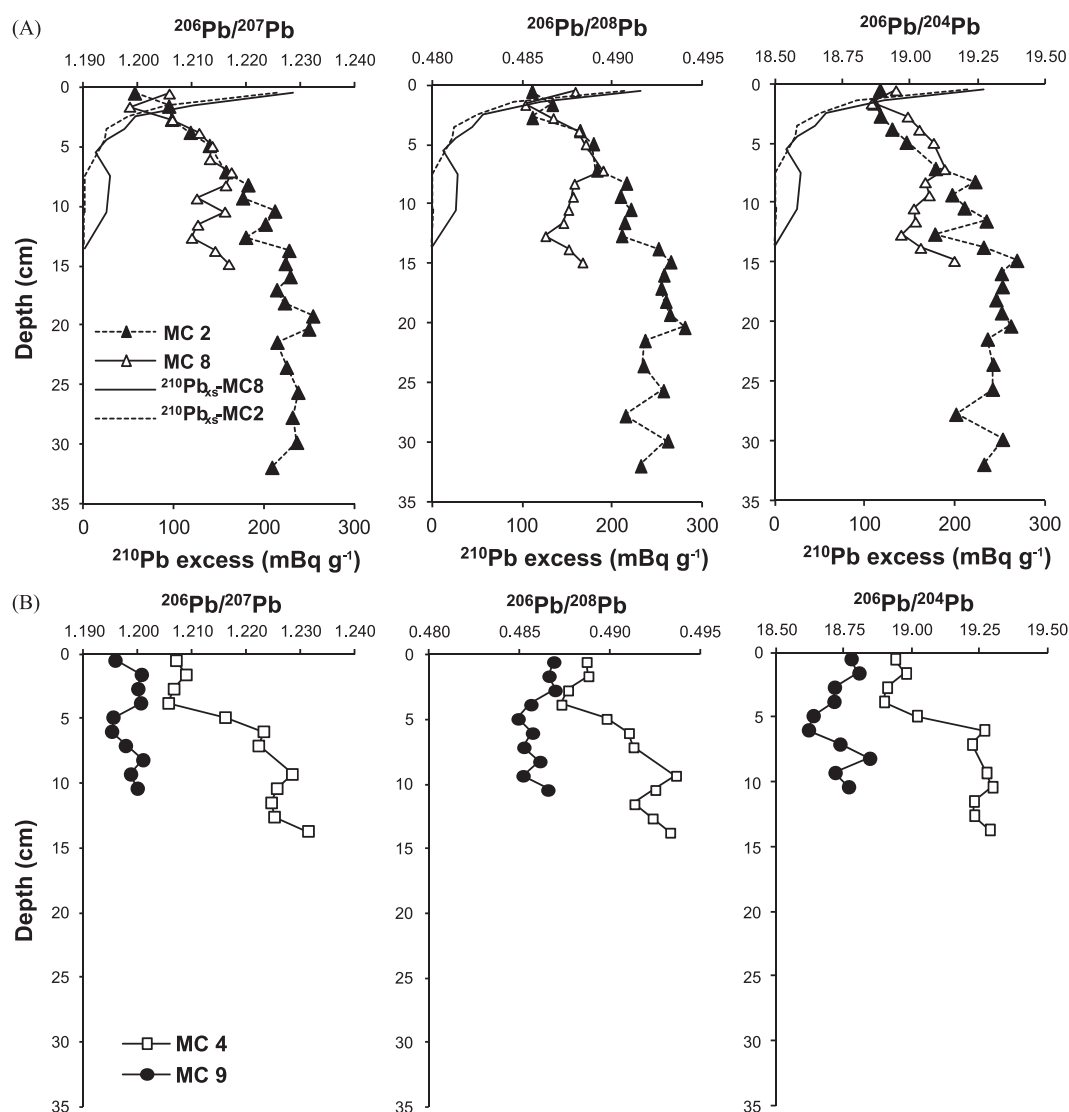
### 3.5. Rare earth elements

Table 2 gives the concentration of each element of the La–Lu series (REE) in the sediment layers of the four cores. High concentrations of total REE ( $\Sigma\text{REE}$ ) were found in cores from the base of the Condor seamount: 91–117  $\mu\text{g g}^{-1}$  in MC2 and 83–102  $\mu\text{g g}^{-1}$  in MC4. As observed for several (Fe, V, Cr, Co, Ni and Cu) low levels of  $\Sigma\text{REE}$  were registered in MC9 (10–20  $\mu\text{g g}^{-1}$ ). Intermediate concentrations were measured in MC8 (71–85  $\mu\text{g g}^{-1}$ ). Lanthanum, Ce and Nd were the most abundant elements, accounting for 75–78% of  $\Sigma\text{REE}$  in MC2, MC4 and MC8 and to 70–74% in MC9. Variability with depth was minor in the four cores. The vertical profiles of the La–Lu series elements were similar in MC4, MC8 and MC9. In core MC2, each REE element profile showed a slight decrease between 9 and 13 cm depth, being values relatively constant in the remain depths (Fig. 1 in Electronic supplementary material).

## 4. Discussion

### 4.1. REE as a proxy of volcanic activity

Levels of La–Lu series elements (REE) obtained in the current study for the base of the Condor and the vicinity area were noteworthy higher than values reported for sites of hydrothermal activity in López-García et al. (2003), Chavagnac et al. (2005) and Dias et al. (2008, 2011). The chondrite-normalized REE (Taylor and McLennan, 1985) in the collected cores are presented in Fig. 6a (MC2, MC4 and MC8) and 6b (MC9). Each core is shown as an area, due to the low variation of REE with depth. Additional



**Fig. 5.** Depth variation of  $^{206}\text{Pb}/^{207}\text{Pb}$ ,  $^{206}\text{Pb}/^{208}\text{Pb}$  and  $^{206}\text{Pb}/^{204}\text{Pb}$  ratios in (a) cores MC2 and MC8 and in (b) cores MC4 and MC9. Excess  $^{210}\text{Pb}$  in cores MC2 and MC8 are also plotted in panel as dashed and solid lines, respectively.

data for pelagic sediments (Wildeman and Haskin, 1965) and volcanic basalts collected in the Capelo volcanic complex and large volcanic fragments extracted from cores MC2 and MC4 are included in Fig. 6a. The distribution pattern found in the base of the Condor seamount and deeper area nearby (MC2, MC4 and MC8) is comparable to volcanic material (basalts and fragments) exhibiting a Light REE (LREE) enrichment in comparison to Heavy REE (HREE). Those three cores showed similar ratios of  $(\text{La}/\text{Yb})_{\text{CH}}$ , 9.3–10.8, differing less from the basalts from Capelo complex (13.0) than the volcanic fragments (5.9) or the pelagic sediments (5.7) reported by Wildeman and Haskin (1965). It should not be excluded the possibility of lower  $(\text{La}/\text{Yb})_{\text{CH}}$  ratio in the volcanic fragments reflect the inclusion of pelagic sediment particles that decreased the ratios due to higher HREE. The lower values of chondrite-normalized REE in the core far away from the Condor (MC8), corroborate the hypothesis of material deposited in the seamount base (MC2 and MC4) being derived from the volcanic activity, either the Condor seamount or the Capelo volcanic complex. Moreover, basalts from this complex showed a  $(\text{La}/\text{Sm})_{\text{CH}}$  ratio of 3.3, which is within the interval found in sediments of this study (3.0–3.4). Although the  $(\text{La}/\text{Sm})_{\text{CH}}$  ratio is less contrasting between pelagic sediments and volcanic material, that similarity is in line with the assumption of particle sources.

Those results are in accordance to Dias et al. (2010) that stated a progressive northwest enrichment of LREE, along the MAR sector with the consequent increase of  $(\text{La}/\text{Sm})_{\text{CH}}$  ratios being as high as 2–3 near the Azores islands. Assuming the relative immobility of La–Lu series elements in material derived from volcanic activity (Zhou et al., 2000) these results point to the benefit of using REE to trace higher contribution of volcanic activities on sediment composition. Normalized REE were much lower in the top of the Condor (MC9), probably reflecting the dilution effect of coarser biogenic carbonates, as reported in previous studies (Araújo et al., 2007; Caetano et al., 2009). In support of this hypothesis is the high variation of the normalized REE with the depth, as observed for Ca and Mg concentrations. Consequently,  $(\text{La}/\text{Yb})_{\text{CH}}$  ratios also showed a broader interval (4.9–9.0). Otherwise, the  $(\text{La}/\text{Sm})_{\text{CH}}$  varied within a narrower interval (2.9–3.6), since both volcanic material and pelagic sedimentary material have comparable ratios (3.0–3.4).

#### 4.2. Anomalies of cerium and europium

Positive or negative deviations, of Ce and Eu from their neighbor pairs of elements are considered as anomalous levels (Elderfield and Graves, 1982; Holser, 1997). The “Ce anomaly”

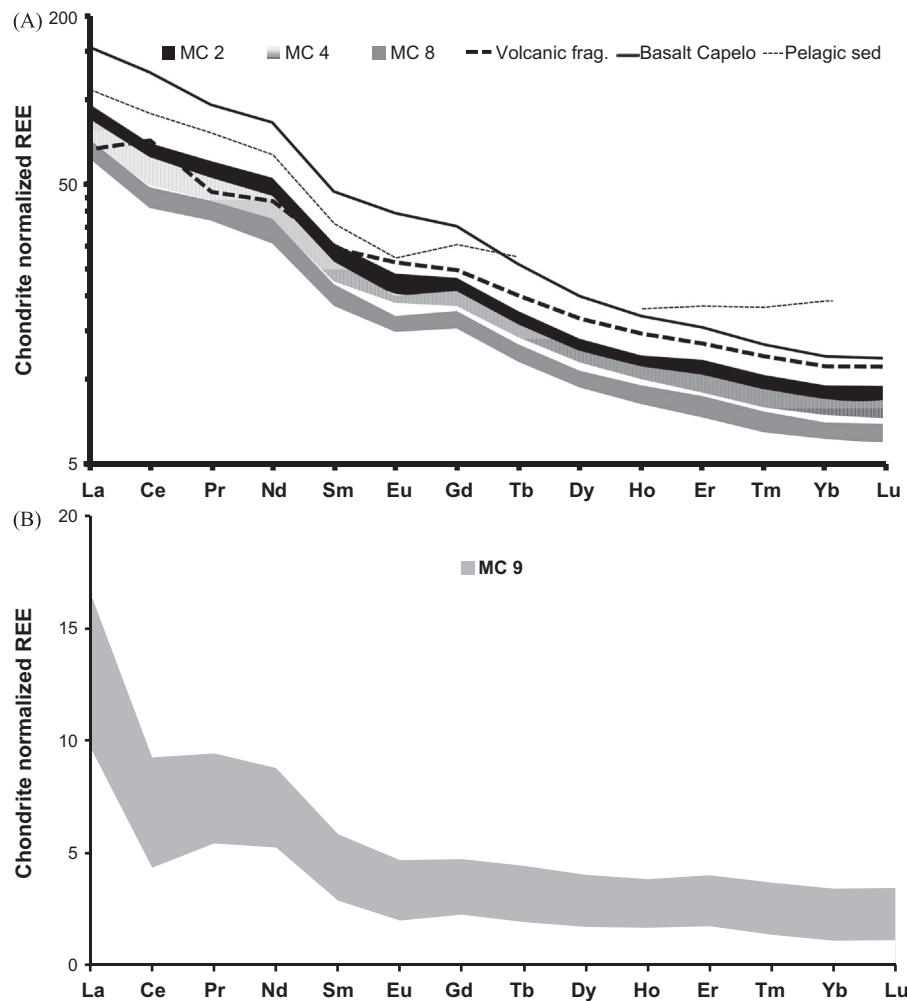


**Fig. 6.** Chondrite normalized REE patterns for the in (a) cores MC2, MC4 (Condor base) and MC8 (far station) and (b) MC9 (top of the seamount). Data from each core is represented as an area that contains all sediment layers. The pattern of volcanic fragments extracted and basalts from volcanic Capelo complex is also presented. Additionally the REE pattern for average pelagic sediments is presented (Wildeman and Haskin, 1965).

and “Eu anomaly” deviations may be calculated by several ways. The formulas most commonly used are:  $Ce/Ce^* = 3(Ce/Ce_{CH}) / (2(La/La_{CH}) + (Nd/Nd_{CH}))$  and  $Eu/Eu^* = (Eu/Eu_{CH}) / ((Sm/Sm_{CH}) \times (Gd/Gd_{CH}))^{1/2}$  (Elderfield and Graves, 1982 and references therein), where the subscript CH means chondrite normalized rare earth element. Sediments of cores MC2, MC4 and MC8 showed a slightly negative Ce anomaly ( $Ce/Ce^* = 0.79\text{--}0.87$ ) compared to the basalt from the Capelo complex ( $Ce/Ce^* = 0.96$ ). The Ce negative anomaly is indicative of post-depositional remobilization of Ce to the water column, while the positive Ce anomaly of the volcanic fragment (1.2) the incorporation of this element from water. No Eu anomaly was found in MC2, MC4 and MC8 cores ( $0.92 \pm 0.04$ ) and in the volcanic material (0.97), since values were closer to the unit.

#### 4.3. Iron and trace elements geochemistry at the Condor area

Table 3 compares the concentration of trace elements in sediments of the current work and other studies in the Azores seafloor. Values of V, Cr, Ni and Co around the Condor seamount base (MC2 and MC4) were lower than nearby hydrothermal hotspots of the region (Cave et al., 2002; Dias et al., 2008, 2011). Metal enrichment in these hotspots was attributed to formation of minerals, such as sulfides that incorporated trace elements from hydrothermal activities (Dias et al., 2010;

Edmonds and German, 2004). Concentrations of those elements in the Condor base exceeded, however, the values reported for sediments far away from areas of documented hydrothermal activities, such as the data obtained during the Biogeochemical Ocean Flux Study (BOFS; Thomson et al., 1993). An additional source of trace elements should be considered to explain the enhanced concentrations in sediments around the Condor seamount. This source should have a local effect since lower concentrations were registered in sediments approximately 10 nm west (MC8). Among the presumable reasons for the enhanced values in MC2 and MC4 is the supply of volcanic material from Condor seamount and from the Capelo volcanic complex that may contain higher trace element concentrations than pelagic sediments. The correlations between V, Cr, Co, Ni and Fe concentrations in cores from Condor base (MC2 and MC4) suggest that trace elements enrichment was associated with the precipitation of Fe insoluble forms. Our results do not allow evaluating which form of sulfides are dominant but the lack of authigenic phase point to volcanoclastic debris. Furthermore, significant correlations ( $p < 0.05$ ) were also found among those trace elements suggesting that they have the same origin. The lack of correlations ( $p > 0.05$ ) between trace elements and Al, Ca or Mg points to the minor role of aluminosilicates or carbonates in the distribution of V, Cr, Co and Ni in this sedimentary environment. These elements in volcanic ashes have minor

Table 2

Rare earth element concentrations in the cores collected in the Condor area, in the basalt from the Capelo Volcanic Complex and in the rock fragment separated from sediment samples.

	La	Ce	Pr	Nd	Sm	Eu	Gd	Tb	Dy ( $\mu\text{g g}^{-1}$ )	Ho	Er	Tm	Yb	Lu	$\Sigma\text{REE}$	Ce/Ce*	Eu/Eu*	(La/Sm) <sub>CH</sub>	(La/Yb) <sub>CH</sub>
<b>MC2 0-1</b>	20	37	4.9	20	4.0	1.3	4.3	0.60	3.2	0.62	1.6	0.22	1.4	0.20	100	0.87	0.96	3.2	10.5
<b>1-2</b>	20	37	5.0	20	4.0	1.3	4.3	0.60	3.3	0.62	1.6	0.22	1.4	0.20	100	0.85	0.94	3.3	10.5
<b>2-3</b>	20	37	4.9	20	4.0	1.3	4.2	0.59	3.2	0.62	1.6	0.22	1.4	0.20	100	0.84	0.94	3.3	10.6
<b>3-4</b>	20	36	4.9	20	3.9	1.3	4.2	0.59	3.2	0.62	1.6	0.22	1.4	0.20	99	0.84	0.95	3.3	10.5
<b>4-5</b>	20	37	4.7	20	3.8	1.2	4.1	0.57	3.1	0.59	1.5	0.21	1.3	0.19	98	0.86	0.94	3.4	11.3
<b>5-6</b>	20	36	4.9	20	3.9	1.3	4.2	0.58	3.2	0.61	1.6	0.22	1.4	0.19	98	0.84	0.94	3.3	10.6
<b>6-7</b>	20	37	4.9	20	3.9	1.2	4.2	0.58	3.2	0.61	1.6	0.22	1.4	0.20	99	0.84	0.95	3.4	10.8
<b>7-8</b>	19	34	4.6	19	3.7	1.2	4.0	0.56	3.0	0.59	1.5	0.21	1.3	0.19	93	0.84	0.93	3.3	10.3
<b>8-9</b>	18	33	4.5	19	3.7	1.2	3.9	0.55	3.0	0.58	1.5	0.21	1.2	0.18	91	0.84	0.94	3.2	10.4
<b>9-10</b>	18	33	4.5	19	3.7	1.2	4.0	0.56	3.0	0.58	1.5	0.21	1.2	0.18	91	0.85	0.93	3.1	10.3
<b>10-11</b>	18	33	4.5	19	3.8	1.2	4.0	0.56	3.0	0.58	1.6	0.21	1.3	0.19	91	0.85	0.94	3.1	10.1
<b>11-12</b>	18	34	4.7	20	3.9	1.3	4.2	0.59	3.2	0.61	1.6	0.21	1.3	0.19	93	0.84	0.96	3.0	9.9
<b>12-13</b>	19	36	4.9	21	4.1	1.3	4.4	0.61	3.3	0.64	1.7	0.23	1.4	0.20	100	0.85	0.94	3.0	10.1
<b>13-14</b>	20	38	5.1	22	4.3	1.4	4.6	0.64	3.4	0.66	1.7	0.23	1.4	0.21	103	0.86	0.95	3.0	10.2
<b>14-15</b>	21	39	5.3	23	4.4	1.4	4.6	0.65	3.5	0.67	1.8	0.24	1.4	0.21	107	0.86	0.94	3.0	10.2
<b>15-16</b>	21	40	5.3	23	4.5	1.4	4.7	0.65	3.5	0.68	1.8	0.24	1.5	0.22	108	0.86	0.93	3.1	10.3
<b>16-17</b>	20	37	5.1	21	4.3	1.4	4.6	0.65	3.5	0.67	1.7	0.23	1.4	0.21	103	0.85	0.97	3.1	10.0
<b>17-18</b>	20	37	5.1	22	4.2	1.3	4.5	0.63	3.4	0.66	1.7	0.23	1.4	0.21	102	0.85	0.94	3.1	10.3
<b>18-19</b>	20	36	5.0	21	4.2	1.4	4.5	0.62	3.4	0.65	1.7	0.23	1.4	0.20	99	0.84	0.96	3.1	10.0
<b>19-20</b>	20	37	5.1	21	4.2	1.4	4.6	0.65	3.5	0.68	1.7	0.23	1.5	0.21	102	0.83	0.96	3.1	10.0
<b>20-22</b>	20	38	5.0	22	4.2	1.3	4.4	0.62	3.3	0.65	1.7	0.23	1.4	0.21	102	0.85	0.93	3.1	10.4
<b>22-24</b>	21	39	5.2	22	4.3	1.3	4.5	0.63	3.4	0.66	1.7	0.24	1.4	0.21	105	0.85	0.93	3.2	10.5
<b>24-26</b>	20	38	5.1	22	4.2	1.4	4.8	0.66	3.6	0.69	1.7	0.24	1.4	0.21	104	0.85	0.95	3.1	10.1
<b>26-28</b>	23	43	5.8	25	4.7	1.4	4.8	0.66	3.6	0.70	2.0	0.27	1.6	0.24	117	0.85	0.90	3.2	10.1
<b>27-28</b>	22	41	5.5	24	4.5	1.4	4.8	0.67	3.6	0.70	1.9	0.25	1.5	0.23	112	0.85	0.92	3.2	10.3
<b>MC4 0-1</b>	-	-	4.4	18	3.6	1.1	3.8	0.53	2.9	0.57	1.5	0.20	1.2	0.18	83	-	0.93	-	-
<b>1-2</b>	-	-	4.5	18	3.6	1.1	3.8	0.54	3.0	0.57	1.5	0.20	1.3	0.18	83	-	0.92	-	-
<b>2-3</b>	18	33	4.4	18	3.6	1.2	4.0	0.55	3.0	0.59	1.5	0.21	1.3	0.19	89	0.85	0.94	3.2	9.8
<b>3-4</b>	18	33	4.4	19	3.6	1.1	3.8	0.53	2.9	0.56	1.5	0.21	1.3	0.19	90	0.85	0.90	3.2	10.1
<b>4-5</b>	19	34	4.6	19	3.8	1.2	4.2	0.58	3.2	0.62	1.6	0.22	1.4	0.20	94	0.85	0.94	3.1	9.7
<b>5-6</b>	20	38	5.0	21	4.1	1.2	4.3	0.59	3.2	0.64	1.7	0.24	1.5	0.22	102	0.86	0.86	3.2	10.0
<b>6-7</b>	19	34	4.6	19	3.8	1.2	4.2	0.58	3.2	0.62	1.6	0.22	1.4	0.20	93	0.84	0.93	3.2	9.7
<b>7-8</b>	18	33	4.5	19	3.7	1.2	4.1	0.57	3.1	0.60	1.6	0.21	1.3	0.19	92	0.84	0.93	3.2	9.8
<b>8-9</b>	17	31	4.3	18	3.5	1.2	4.0	0.56	3.1	0.59	1.5	0.20	1.3	0.19	86	0.83	0.95	3.2	9.6
<b>9-10</b>	-	-	4.6	19	3.8	1.2	4.0	0.56	3.1	0.60	1.6	0.21	1.3	0.19	86	-	0.93	-	-
<b>10-11</b>	18	33	4.6	19	3.8	1.2	4.2	0.59	3.3	0.63	1.6	0.22	1.4	0.20	92	0.83	0.94	3.1	9.4
<b>11-12</b>	17	31	4.2	17	3.5	1.1	3.8	0.54	3.0	0.58	1.5	0.21	1.3	0.19	84	0.84	0.93	3.1	9.3
<b>12-13</b>	18	33	4.6	19	3.8	1.2	4.2	0.58	3.2	0.62	1.6	0.22	1.4	0.20	92	0.84	0.93	3.2	9.5
<b>13-15.5</b>			4.8	20	3.9	1.2	4.1	0.58	3.2	0.62	1.6	0.22	1.4	0.20	90	-	0.92	-	-
<b>MC8 0-1</b>	17	29	4.0	16	3.2	0.99	3.6	0.49	2.7	0.53	1.4	0.19	1.2	0.17	80	0.80	0.90	3.4	10.2
<b>1-2</b>	17	28	4.0	16	3.2	1.0	3.6	0.50	2.8	0.53	1.4	0.19	1.2	0.17	80	0.80	0.90	3.3	10.1
<b>2-3</b>	16	29	4.0	17	3.2	0.94	3.5	0.48	2.6	0.52	1.4	0.19	1.2	0.17	80	0.80	0.87	3.3	10.2
<b>3-4</b>	15	25	3.5	14	2.8	0.87	3.2	0.44	2.4	0.47	1.2	0.17	1.1	0.15	71	0.79	0.89	3.4	10.0
<b>4-5</b>	18	30	4.2	18	3.4	0.96	3.5	0.49	2.7	0.53	1.5	0.20	1.2	0.18	85	0.80	0.84	3.4	10.2
<b>5-6</b>	16	28	3.9	17	3.2	0.96	3.6	0.49	2.7	0.53	1.4	0.19	1.2	0.17	79	0.80	0.87	3.3	10.1
<b>6-7</b>	17	30	4.1	17	3.3	0.95	3.5	0.49	2.7	0.53	1.4	0.19	1.2	0.17	83	0.80	0.85	3.4	10.4
<b>7-8</b>	17	30	4.1	17	3.3	0.96	3.6	0.49	2.7	0.53	1.4	0.20	1.2	0.18	83	0.80	0.85	3.3	10.4
<b>8-9</b>	17	30	4.2	18	3.4	0.99	3.6	0.51	2.8	0.55	1.5	0.20	1.2	0.18	84	0.80	0.86	3.3	10.2
<b>9-10</b>	17	29	4.1	17	3.3	0.98	3.6	0.50	2.7	0.54	1.4	0.20	1.2	0.18	82	0.80	0.86	3.2	10.0
<b>10-11</b>	16	29	4.0	17	3.3	0.96	3.5	0.49	2.7	0.53	1.4	0.19	1.2	0.17	81	0.80	0.86	3.2	10.0
<b>11-12</b>	17	29	4.0	17	3.3	0.96	3.5	0.49	2.7	0.53	1.4	0.19	1.2	0.17	81	0.80	0.86	3.2	10.1
<b>12-13</b>	17	29	4.1	17	3.3	0.96	3.6	0.49	2.7	0.53	1.5	0.20	1.2	0.18	82	0.80	0.85	3.3	10.1
<b>13-14</b>	15	26	3.7	15	3.0	0.94	3.4	0.47	2.6	0.50	1.3	0.18	1.1	0.16	73	0.79	0.89	3.2	9.7

Table 2 (continued)

	La	Ce	Pr	Nd	Sm	Eu	Gd	Tb	Dy ( $\mu\text{g g}^{-1}$ )	Ho	Er	Tm	Yb	Lu	$\Sigma\text{REE}$	Ce/Ce*	Eu/Eu*	(La/Sm) <sub>ch</sub>	(La/Yb) <sub>ch</sub>
MC9 0–1	2.6	3.1	0.54	2.4	0.46	0.13	0.52	0.084	0.52	0.11	0.33	0.045	0.27	0.042	11	0.58	0.80	3.6	6.7
1–2	2.9	3.7	0.64	2.9	0.56	0.15	0.61	0.10	0.61	0.13	0.39	0.052	0.28	0.044	13	0.58	0.79	3.3	7.4
2–3	2.9	3.4	0.63	2.9	0.54	0.14	0.57	0.091	0.56	0.12	0.37	0.047	0.26	0.040	13	0.55	0.79	3.4	7.9
3–4	2.3	2.7	0.50	2.4	0.43	0.12	0.46	0.072	0.43	0.093	0.28	0.034	0.18	0.028	10	0.55	0.80	3.4	9.1
4–5	3.4	4.3	0.75	3.4	0.68	0.19	0.75	0.12	0.77	0.17	0.52	0.071	0.44	0.066	16	0.59	0.83	3.2	5.6
5–6	2.4	2.9	0.54	2.6	0.46	0.12	0.48	0.075	0.44	0.096	0.29	0.035	0.19	0.029	11	0.54	0.79	3.4	9.3
6–7	3.4	4.3	0.74	3.3	0.66	0.18	0.72	0.12	0.74	0.16	0.51	0.072	0.46	0.069	15	0.58	0.80	3.3	5.4
7–8	3.9	5.7	0.89	4.1	0.89	0.27	1.0	0.16	1.0	0.22	0.66	0.093	0.58	0.087	20	0.66	0.89	2.9	4.9
8–9	3.7	4.3	0.80	3.6	0.73	0.20	0.79	0.13	0.83	0.18	0.59	0.082	0.50	0.077	17	0.55	0.80	3.3	5.3
9–10	2.3	2.7	0.51	2.4	0.44	0.11	0.46	0.071	0.43	0.093	0.28	0.034	0.18	0.028	10	0.53	0.78	3.4	9.1
Basalt Capelo	37	77	9.1	39	7.2	2.3	7.3	0.97	5.1	0.96	2.6	0.34	2.1	0.31	190	0.96	0.97	3.3	13
Rock fragment	16	44	4.5	20	4.6	1.5	5.1	0.76	4.3	0.84	2.3	0.31	1.9	0.29	107	1.22	0.98	2.2	5.9

post-depositional mobility due to early diagenesis, being preserved in sediment (Burdige 2006; Zhou et al., 2000). It should not be excluded the existing small-scale hydrothermal zones in the area (Giovannelli et al., 2012) providing particles enriched in Fe and other trace elements that dispersed in the water column and ultimately settle on the bottom. If this hypothesis is realistic, releases should have occurred for decades to account the relative uniform composition of sediments with depth. The region is located at the tectonic Azores Triple Junction on the Mid-Atlantic Ridge where hydrothermal activity is intense (Cannat et al., 1999; Rona et al., 1986). However, it is unknown the extent and the impact of hydrothermal fluids on the adjacent non-hydrothermal ecosystems such as the seamounts and islands slopes. The similar concentrations of either Mn or Cu in the cores MC2, MC4 and MC8 indicate that those elements have not an additional source near the Condor seamount.

The minor increase of V, Co, Cr and Ni in the topmost sediment layer of MC2, MC4 MC8 implies the settling of biogenic detritus containing these elements. The low organic matter content in sediments ensure that oxic conditions prevail in bottom sediments and these elements are released to the pore water upon organic matter degradation (Gobeil et al., 1987; Shaw et al., 1990). In MC8 no depth enrichment was found indicating the lack of authigenic phases to deep burial of those trace elements in the sedimentary environment, thus, promoting their upward diffusion back to the water column (Calvert and Pedersen, 1993; Shaw et al., 1990; Sundby et al., 2004). The same process should have been occurred in MC4 and MC2 sediments since variations of V, Co, Cr and Ni are presumably related with input of volcanic material. The lack of surface enrichment for Cu and As suggest that both elements are preferentially mobilized in the water column, as material derived from biological production, or in the sediment–water interface through aerobic oxidation of organic material (Shaw et al., 1990).

#### 4.4. Elevated cadmium and arsenic concentrations

The core collected at the top of the Condor seamount (MC9) was characterized by higher concentrations of carbonates, Ca, Cd and As than in other cores. Furthermore, values varied within broad intervals in the sediment column, pointing to either an irregular supply of these elements to the sediment with time or internal post-remobilisation. The strong positive correlation between Cd and Ca ( $r=0.805$ ,  $p < 0.01$ ) points to the retention of this trace element in the carbonate phase of the sediment, which is mainly formed by calcite. The presence of fauna debris along the core seems to indicate that calcite enrichment is related to fragments derived from pelagic and benthic organisms. It should not be discarded the possibility of post-deposition precipitation of carbonates. This explanation is not extended to As since no significant correlation was found between As and Ca. Nevertheless, As concentration is comparable to values reported in the Rainbow vent field (Cave et al., 2002), strengthening the hypothesis of an additional local source. The enrichment of Cd and As in sediments is in line with observation of high concentrations in corals and fish tissues (Raimundo et al., 2013-a,b) sampled at the Condor seamount. Bioaccumulation of these elements through water and suspended particulate matter reinforces the hypothesis of a local source of Cd and As in the Condor marine environment.

#### 4.5. Record of Pb in the environment

The sedimentation rates estimated for MC2 and MC8 (0.059 and 0.063  $\text{cm yr}^{-1}$ ) were up to five times higher than the average value found in the literature ( $0.0098 \pm 0.0045 \text{ cm yr}^{-1}$ ) for ocean

**Table 3**  
Ranges of trace metal concentrations ( $\mu\text{g g}^{-1}$ ) in sediments from the present study and from the literature.

Sample	Site	V	Cr	Ni	Co	Cu ( $\mu\text{g g}^{-1}$ )	As	Cd	Pb	Reference
Sediment	Condor seamount	17–106	8–67	12–42	2–16	4–29	5–21	0.2–0.6	3–9	Present study
Sediment	Rainbow vent	31–129	8–139	10–85		73–448	7–39			Cave et al. (2002)
Sediment	32°53.5'N 19°16.4'W	26–33	19–28	13		19–47	<1			Cave et al. (2002)
Serpentinite	Rainbow vent	54	977	1490		116	45			Cave et al. (2002)
Sediment	Lucky Strike Hydrothermal field	303–380	167–522	16–57	41–152	1850–7850	22–100	237–392	69–263	Dias et al. (2008)
Sediment	Saldanha hydrothermal field	28–489	10–3290	9–105	13–1850	22–1240				Dias et al. (2011)
Sediment	Away from vent areas (MAR)	8–165	2–16	8–40	6–21	18–116				Dias et al. (2011)

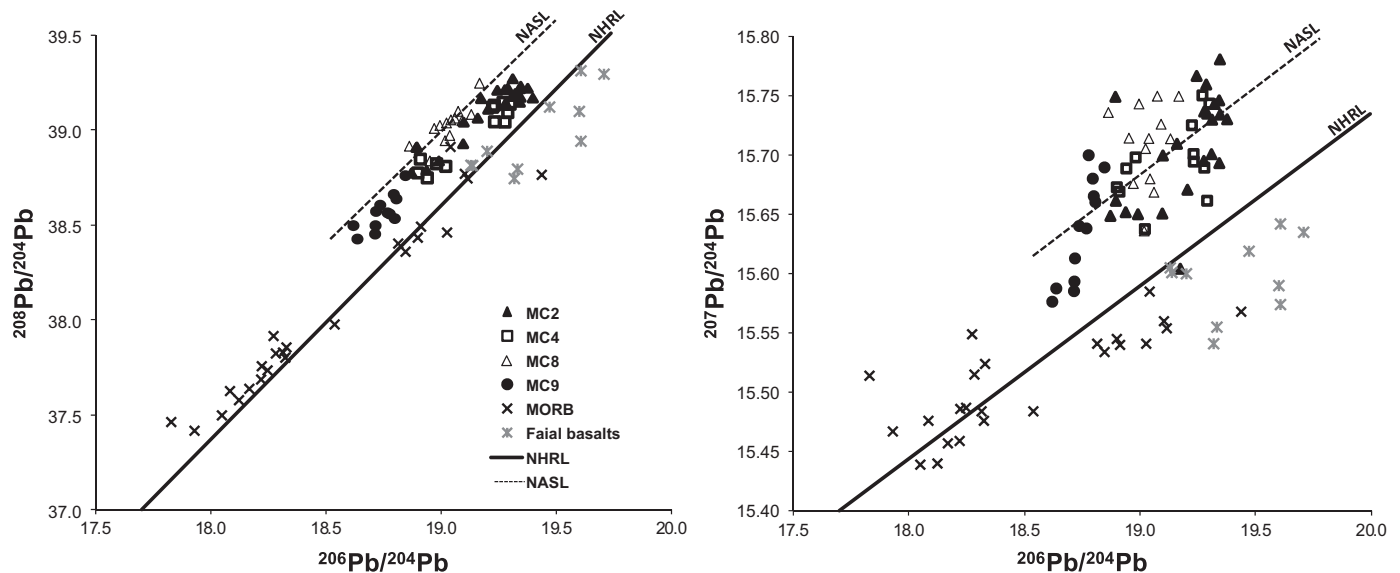


**Fig. 7.** Plots of  $^{206}\text{Pb}/^{204}\text{Pb}$  vs.  $^{208}\text{Pb}/^{204}\text{Pb}$  and  $^{206}\text{Pb}/^{204}\text{Pb}$  vs.  $^{207}\text{Pb}/^{204}\text{Pb}$  for the two cores collected in the Condor base (MC2 and MC4), one in the top of the seamount (MC9) and other far from it (MC8). Data from MORB (Ito et al., 1987) and Faial basalts (Moreira et al., 1999) were also projected, as well as values for North Atlantic Sediment Line (NASL, Othman et al., 1989) and North Hemisphere Reference Line (NHRL, Hart, 1984).

sediments (Boudreau, 1994, 1998; Thomson et al., 2000). Enhanced sedimentation rates may reproduce weathering processes of the Condor seamount and islands and or input of volcanoclastic debris from nearby volcanic activities that contribute to material input to the seabed.

Profiles of  $^{210}\text{Pb}$  alone do not allow distinguishing between sedimentation and bioturbation processes (Angelidis et al., 2011; Crusius and Kenna, 2007). However,  $^{137}\text{Cs}$  profiles showed a rapid decrease within the upper 3–5 cm of cores MC2 and MC8, arguing in favor of a dominant sedimentation processes. According to Thomson et al. (2000) the simplest and most widely used treatment of excess  $^{210}\text{Pb}$  data assumes that bioturbative mixing occurs as a large number of small-scale events that may be modeled by analogy with a diffusion process. The depth penetration of excess  $^{210}\text{Pb}$  (i.e. 6 cm, Fig. 4) provides an age constraint of 100–150 yr for particles accumulated within the top sequence of cores. The similarity of the upper sediment layers of the two cores indicates that they are representative of the mean sedimentation-mixing processes occurring in the Condor and surrounding area. In fact, the linear decrease from topmost layer of Pb concentrations and the increasing tendency of stable Pb isotopes ratios with depth mirrors these processes. Assuming similar sedimentation rates in MC2 and MC4 the gradual decrease of Pb isotopic ratios until 6-cm depth results from the bioturbative mixing of anthropogenic Pb with low radiogenic signature (Alleman et al., 1999; Gobeil et al., 2001) from the surface to deeper layers. The isotopic Pb signature found in surface sediments from the Condor and

surrounding area is similar to values of North Atlantic Deep Water (Alleman et al., 1999; Muñoz et al., 2008). Based on Pb profiles in MC2 and MC4 we established a baseline total Pb concentration of  $3.6 \pm 0.2 \mu\text{g g}^{-1}$  for those sediments with  $^{206}\text{Pb}/^{207}\text{Pb} = 1.227 \pm 0.003$  and  $^{206}\text{Pb}/^{208}\text{Pb} = 0.492 \pm 0.001$  signature. The increased  $^{210}\text{Pb}$  activities in deeper layers of core far away from the Condor (MC8) indicate that it is affected by non-diffusive bioturbation (Boudreau, 1986). This non-local mixing may derive from worm species that transport water and particles from surface to deeper layers (Thomson et al., 2000). In fact, the clear peak of Mn concentration in this sediment layer is indicative of bioirrigation presumably as overlying oxygenated water is injected in deeper suboxic sediments inducing the generation of Mn oxyhydroxides (Aller, 1977). Furthermore, this mixing had transported anthropogenic Pb to deeper sediments not allowing the evaluation of the background levels and Pb isotopic signature in this core. Sediments from the top of the seamount (MC9) evidence a different pattern with relatively constant isotopic signature closer to values found in NADW ( $1.175 < ^{206}\text{Pb}/^{207}\text{Pb} < 1.210$ , Alleman et al., 1999) suggesting a different environmental setting (hydrothermal contributions, high energetic conditions and increased benthonic activity) that imprints a different geochemical signature to the sediments.

The distribution of Pb isotopic ratios is plotted on conventional inter-isotopic ratio diagrams (Fig. 7) containing reference values of the North Hemisphere Reference Line (NHRL, Hart, 1984), North Atlantic Sediment Line defined by Pb isotopic ratios of

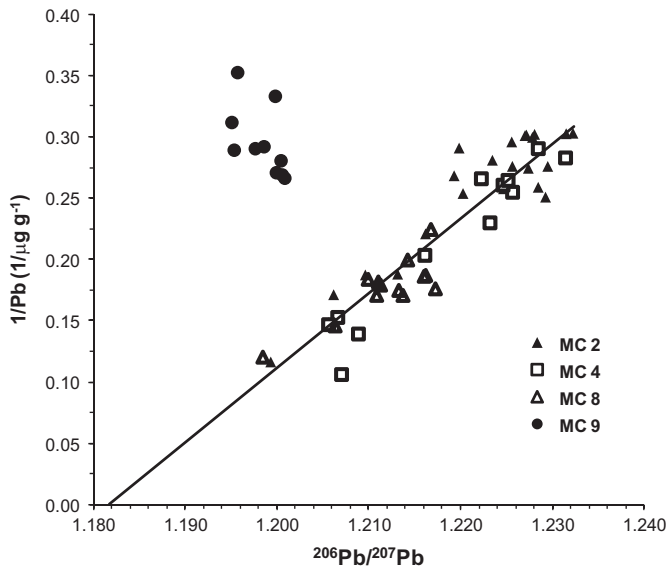


**Fig. 8.** Ratios of  $^{206}\text{Pb}/^{207}\text{Pb}$  in sediments (MC2, MC4, MC8 and MC9) plotted against the inverse of Pb concentration. Samples from MC9 (filled circles) with anomalously low Pb levels were excluded from calculation of regression line.

pelagic, terrigenous and biogenic Atlantic sediments (NASL; Othman et al., 1989). Data from Mid-Ocean Reference Basalts (MORB, Ito et al., 1987) and from basalts of the volcanic complexes in Faial Island (Moreira et al., 1999) were also used for comparison. The Pb isotopic composition of sediments from the Condor falls closer to NASL, away from the NHRL. Sediments also showed a  $^{206}\text{Pb}/^{204}\text{Pb}$  signature closer to basalts of the Capelo volcanic complexes than from MORB. These results suggest that similar geological formations contribute to the sediment from the Condor area. The almost linear distribution of data in the  $^{208}\text{Pb}/^{204}\text{Pb}$  vs.  $^{206}\text{Pb}/^{204}\text{Pb}$  plot points that Pb in this environment can be described as a mixture of more radiogenic Pb (background) with less radiogenic Pb values (indicative of more anthropogenic contributions), assuming the absence of significant changes of environmental conditions through time. On the basis of this mixing the isotopic composition of the anthropogenic end member can be estimated from the x-axis intercept of  $^{206}\text{Pb}/^{207}\text{Pb}$  vs. the inverse of the Pb concentration ( $r=0.951$ ;  $p < 0.05$ ; Fig. 8). This yields  $^{206}\text{Pb}/^{207}\text{Pb}$  ratios of 1.182 for the data set of MC2, MC4 and MC8 cores excluding values from core MC9 that displays low  $^{206}\text{Pb}/^{207}\text{Pb}$  ratio for a given concentration (see also Figs. 4 and 5). Presumably the low  $^{206}\text{Pb}/^{207}\text{Pb}$  ratios in sediments from MC9 core follows near the basalts field, suggesting a similar rock source as a result of weathering of basaltic formations. The anthropogenic Pb component is comparable with the isotopic signature reported by Véron and Church (1997) in air samples ( $1.1837 \pm 0.0004$ ) collected in the central Atlantic suggesting a direct atmospheric impact of anthropogenically derived aerosols on deposited sediments. Moreover,  $^{206}\text{Pb}/^{207}\text{Pb}$  ratios falls within the range observed in North Atlantic surface waters (1.1810–1.1913) (Véron et al., 1994).

## 5. Conclusions and final remarks

Condor Seamount appears to constitute an additional source of trace and rare earth elements to the surrounded sediments, either due to weathering of the slopes or associated with the existence of possible hydrothermal activity. Furthermore, the spatial distribution of REE in sediments highlights the use of La–Lu series elements as a proxy for volcanic activities. Metal enrichments in

sediments closer to the Capelo volcanic complex seem to be mainly due to the input of volcanoclastic debris than promoted by diagenesis. Enhanced Pb concentrations and low radiogenic signature of stable Pb isotopes were registered in the surface sediment layers. Lead isotopic signature in surface sediments is comparable to values found in the North Atlantic Deep Water. Besides anthropogenic signal due to global increase of Pb in the last century, bioturbation mixing may also have occurred.

## Acknowledgments

The authors would like to thank all participants in the Condor 2010 cruise for various forms of indispensable cooperation in sampling and R. Medeiros<sup>©</sup>ImagDOP the map design. The current work was supported by a grant from Iceland, Liechtenstein and Norway through the EEA Financial Mechanism—Project CONDOR (PT0040).

## Appendix A. Supplementary material

Supplementary data associated with this article can be found in the online version at <http://dx.doi.org/10.1016/j.dsr2.2013.01.009>.

## References

- Alleman, L., Véron, A., Church, T., Flégal, A., Hamelin, B., 1999. Invasion of the abyssal North Atlantic by modern anthropogenic lead. *Geophys. Res. Lett.* 26, 1477–1480.
- Aller, R., 1977. The Influence of Macrobenthos on Chemical Diagenesis of Marine Sediments. Ph.D. Thesis. Yale University.
- Angelidis, M., Radakovitch, O., Véron, A., Aloupi, M., Heussner, S., Price, B., 2011. Anthropogenic metal contamination and sapropel imprints in deep Mediterranean sediments. *Mar. Pollut. Bull.* 62, 1041–1052.
- Araújo, M.F., Corredeira, C., Gouveia, A., 2007. Distribution of rare elements in sediments of the Northwestern Iberian Continental Shelf. *J. Radioanal. Nucl. Chem.* 271, 255–260.
- Berner, R., 1980. *Early Diagenesis. A Theoretical Approach*. Princeton University Press, USA.
- Boström, K., Peterson, S., 1969. The origin of aluminium-poor ferromanganese sediments in areas of areas of high heat flow on the East Pacific Rise. *Mar. Geol.* 7, 427–447.
- Boudreau, B.P., 1986. Mathematics of tracer mixing in sediments: II. Nonlocal mixing and biological conveyor-belt phenomena. *Am. J. Sci.* 268, 199–238.
- Boudreau, B.P., 1994. Is burial velocity a master parameter for bioturbation? *Geochim. Cosmochim. Acta* 58, 1243–1249.
- Boudreau, B., 1998. Mean mixed depth of sediments: the wherefore and the why. *Limnol. Oceanogr.* 43, 524–526.
- Burdige, D.J., 2006. *Geochemistry of Marine Sediments*. Princeton University Press, USA.
- Caetano, M., Fonseca, N., Cesário, R., Vale, C., 2007. Mobility of Pb in salt marshes recorded by total content and stable isotopic signature. *Sci. Total Environ.* 380, 93–101.
- Caetano, M., Prego, R., Vale, C., de-Pablo, H., Marmolejo-Rodríguez, J., 2009. Evidence for early diagenesis of rare earth elements and metals in a transition sedimentary environment. *Mar. Chem.* 116, 36–46.
- Calvert, S.E., Pedersen, T.F., 1993. Geochemistry of recent oxic and anoxic marine sediments: implications for the geological record. *Mar. Geol.* 113, 67–88.
- Cannat, M., Briais, A., Deplus, C., Escartin, J., Georgen, J., Lin, J., Mercouriev, S., Meyzen, C., Muller, M., Pouliquen, G., Rabain, A., Silva, P., 1999. Mid-Atlantic Ridge–Azores hotspot interactions: along-axis migration of a hotspot-derived event of enhanced magmatism 10 to 4 Ma ago. *Earth Planet. Sci. Lett.* 173, 257–269.
- Cave, R.R., German, C.R., Thomson, J., Nesbitt, R.W., 2002. Fluxes to sediments underlying the Rainbow hydrothermal plume at 36°14'N on the Mid-Atlantic Ridge. *Geochim. Cosmochim. Acta* 66, 1905–1923.
- Chavagnac, V., German, C., Milton, J., Palmer, M., 2005. Sources of REE in sediment cores from the Rainbow vent site (36°14'N, MAR). *Chem. Geol.* 216, 329–352.
- Crusius, J., Kenna, T., 2007. Ensuring confidence in radionuclide-based sediment chronologies and bioturbation rates. *Estuarine Coastal Shelf Sci.* 71, 537–544.
- Dias, Á.S., Barriga, F.J.A.S., 2006. Mineralogy and geochemistry of hydrothermal sediments from the serpentinite-hosted Saldanha hydrothermal field (36°34'N; 33°26'W) at MAR. *Mar. Geol.* 225, 157–175.
- Dias, Á.S., Mills, R.A., Taylor, R.N., Ferreira, P., Barriga, F.J.A.S., 2008. Geochemistry of a sediment push-core from the Lucky Strike Hydrothermal field, Mid-Atlantic Ridge. *Chem. Geol.* 247, 339–351.

- Dias, Á.S., Mills, R.A., Ribeiro da Costa, I., Costa, R., Taylor, R.N., Cooper, M.J., Barriga, F.J.A.S., 2010. Tracing fluid–rock reaction and hydrothermal circulation at the Saldanha hydrothermal field. *Chem. Geol.* 273, 168–179.
- Dias, Á.S., Früh-Green, G., Bernasconi, S., Barriga, F., Seahma cruise team, Charles Darwin 167 cruise team, 2011. Geochemistry and stable isotope constraints on high-temperature activity from sediment cores of the Saldanha hydrothermal field. *Mar. Geol.* 279, 128–140.
- Dias, J.M.A., 1987. Dinâmica sedimentar e evolução recente da plataforma continental portuguesa setentrional. Ph.D. Thesis. University of Lisbon.
- Dosso, L., Bougault, H., Langmuir, C., Bollinger, C., Bonnier, O., Etoubleau, J., 1999. The age and distribution of mantle heterogeneity along the Mid-Atlantic Ridge (31°–41°N). *Earth Planet. Sci. Lett.* 170, 269–286.
- Douville, E., Charlou, J.L., Oelkers, E.H., Bienvenu, P., Jove-Colon, C.F., Donval, J.P., Fouquet, Y., Prieur, D., Appriou, P., 2002. The Rainbow vent fluids (36°14'N, MAR): the influence of ultramafic rocks and phase separation on trace metal content in Mid-Atlantic Ridge hydrothermal fluids. *Chem. Geol.* 184, 37–48.
- Edmonds, H., German, C., 2004. Particle geochemistry in the Rainbow hydrothermal plume, Mid-Atlantic Ridge. *Geochim. Cosmochim. Acta* 68, 759–772.
- Elderfield, H., Graves, M., 1982. The rare earth elements in seawater. *Nature* 269, 214–219.
- Flemming, B., 2000. A revised textural classification of gravel-free muddy sediments on the basis of ternary diagrams. *Cont. Shelf Res.* 20, 1125–1137.
- Giovannelli, D., Grosche, A., Starovoytov, V., Yakimov, M., Manini, E., Vetriani, C., 2012. *Galenea microaerophila* gen. nov., sp. nov., a mesophilic, microaerophilic, chemosynthetic, thiosulfate-oxidizing bacterium isolated from a shallow water hydrothermal vent. *International Journal of Systematic and Evolutionary Microbiology* 62, 3060–3066.
- Gobeil, C., Silverberg, N., Sundby, B., Cossa, D., 1987. Cadmium diagenesis in Laurentian Trough sediments. *Geochim. Cosmochim. Acta* 51, 589–596.
- Gobeil, C., MacDonald, R., Smith, J., Beaudin, L., 2001. Atlantic water flow pathways revealed by lead contamination in arctic basin sediments. *Science* 293, 1301–1304.
- Hamelin, B., Dupre, B., Allegre, C.J., 1984. Lead–strontium isotopic variations along the East Pacific Rise and the Mid-Atlantic Ridge: a comparative study. *Earth Planet. Sci. Lett.* 67, 340–350.
- Hart, S.R., 1984. A large-scale isotope anomaly in the Southern Hemisphere mantle. *Nature* 309, 753–757.
- Henderson, G., Maier-Reimer, E., 2002. Advection and removal of <sup>210</sup>Pb and stable Pb isotopes in the oceans: a general circulation model study. *Geochim. Cosmochim. Acta* 66, 257–272.
- Holser, W.T., 1997. Evaluation of the application of rare-earth elements to paleoceanography. *Palaeogeogr. Palaeoclimatol. Palaeoecol.* 132, 309–323.
- Hu, Z., Gao, S., 2008. Upper crustal abundances of trace elements: a revision and update. *Chem. Geol.* 253, 205–221.
- Ito, E., White, W., Gopel, C., 1987. The O, Sr, Nd and Pb isotope geochemistry of MORB. *Chem. Geol.* 62, 157–176.
- López-García, P., Philippe, H., Gail, F., Moreira, F., 2003. Autochthonous eukaryotic diversity in hydrothermal sediment and experimental microcolonizers at the Mid-Atlantic Ridge. *Proc. Natl. Acad. Sci.* 100, 697–702.
- Lourenço, N., Miranda, J., Luís, J., Ribeiro, A., Victor, L., Madeira, J., Needham, H.D., 1998. Morpho-tectonic analysis of the Azores Volcanic Plateau from a new bathymetric compilation of the area. *Mar. Geophys. Res.* 20, 141–156.
- Marques, A., Barriga, F., Scott, S., 2007. Sulfide mineralization in an ultramafic-rock hosted seafloor hydrothermal system: from serpentinization to the formation of Cu–Zn–(Co)-rich massive sulphides. *Mar. Geol.* 245, 20–39.
- Mascarenhas-Pereira, M.B., Nath, B.N., Borole, D.V., Gupta, S.M., 2006. Nature, source and composition of volcanic ash in sediments from a fracture zone trace of Rodriguez Triple Junction in the Central Indian Basin. *Mar. Geol.* 229, 79–90.
- Mills, R.A., Elderfield, H., 1995. Hydrothermal activity and the geochemistry of metalliferous sediments. *Amer. Geophys. Union* 91, 392–407.
- Morford, J.L., Emerson, S., 1999. The geochemistry of redox sensitive trace elements in sediments. *Geochim. Cosmochim. Acta* 63, 1735–1750.
- Moreira, M., Doucelance, R., Kurz, M., Dupré, B., Allègre, C., 1999. Helium and lead isotope geochemistry of the Azores Archipelago. *Earth Planet. Sci. Lett.* 169, 189–205.
- Muiños, S., Frank, M., Maden, C., Hein, J., van de Fliedert, T., Lebreiro, S., Gaspar, L., Monteiro, J., Halliday, A., 2008. New constraints on the Pb and Nd isotopic evolution of NE Atlantic water masses. *Geochem. Geophys. Geosyst.* 9, Q02007.
- Oliveira, A., Vitorino, J., Rodrigues, A., 2007. Sedimentary particle distribution and dynamics on the Nazaré canyon system and adjacent shelf (Portugal). *Mar. Geol.* 246, 105–122.
- Othman, D., White, W., Patchett, J., 1989. The geochemistry of marine sediments, island arc magma genesis, and crust–mantle recycling. *Earth Planet. Sci. Lett.* 94, 1–21.
- Raimundo, J., Vale, C., Caetano, M., Anes, B., Porteiro, F., Silva, M., 2013a. Element concentrations in deep-sea gorgonians and black coral from Azores Archipelago. *Deep-Sea Res.* 98 (PA), 129–136.
- Raimundo, J., Anes, B., Caetano, M., Giacomello, E., Menezes, G., Vale, C., 2013b. Trace-element concentrations in muscle and liver of 11 commercial fish species from Condor Seamount, Azores Archipelago (Portugal). *Deep-Sea Res.* 98 (PA), 137–147.
- Rantala, R., Loring, D., 1975. Multi-element analysis of silicate rocks and marine sediments by atomic absorption spectrophotometry. *At. Absorpt. Newsl.* 14, 117–120.
- Reuer, M., Boyle, E., Grant, B., 2003. Lead isotope analysis of marine carbonates and seawater by multiple collector ICP-MS. *Chem. Geol.* 200, 137–153.
- Robbins, J., Edgington, D.N., 1975. Determination of recent sedimentation rates in Lake Michigan using <sup>210</sup>Pb and <sup>137</sup>Cs. *Geochim. Cosmochim. Acta* 39, 285–304.
- Rona, P.A., Klinkhammer, G., Nelsen, T.A., Trefry, J.H., Elderfield, H., 1986. Black smokers, massive sulphides and vent biota at the Mid-Atlantic Ridge. *Nature* 321, 33–37.
- Santos, I.R., Fávoro, D.I.T., Schaefer, C.E.G.R., Silva-Filho, E.V., 2007. Sediment geochemistry in coastal maritime Antarctica (Admiralty Bay, King George Island): evidence from rare earths and other elements. *Mar. Chem.* 107, 464–474.
- Schmidt, S., Jouanneau, J.M., Weber, O., Lacroart, P., Radakovitch, O., Gilbert, F., Jezequel, D., 2007. Sedimentary processes in the Thau Lagoon (South France): from seasonal to century time scales. *Estuarine, Coastal Shelf Sci.* 72, 534–542.
- Shaw, T., Gieskes, J., Jahnke, R., 1990. Early diagenesis in different depositional environments: the response of transition metals in pore water. *Geochim. Cosmochim. Acta* 54, 1233–1246.
- Smirnova, E.V., Fedorova, I.N., Sandimirova, G.P., Petrov, L.L., Balbekina, N.G., Lozhkin, V.I., 2003. Determination of rare earth elements in black shales by inductively coupled plasma mass spectrometry. *Spectrochim. Acta Part B* 58, 329–340.
- Sundby, B., Martinez, P., Gobeil, C., 2004. Comparative geochemistry of cadmium, rhenium, uranium, and molybdenum in continental margin sediments. *Geochim. Cosmochim. Acta* 68, 2485–2493.
- Taylor, S.R., McLennan, S.M., 1985. *The Continental Crust: Its Composition and Evolution*. Blackwell, Oxford.
- Tempera, F., Giacomello, E., Mitchell, N., Campos, A., Henriques, A., Bashmachnikov, I., Martins, A., Mendonça, A., Morato, T., Colaço, A., Porteiro, F., Catarino, D., Gonçalves, J., Pinho, M., Isidro, E., Santos, R., Menezes, G., 2012. Mapping Condor seamount seafloor environment and associated biological assemblages (Azores, NE Atlantic). In: Harris, P., Baker, E. (Eds.), *Seafloor Geomorphology as Benthic Habitat*. *GeoHAB Atlas of Seafloor Geomorphic Features and Benthic Habitats*. Elsevier, USA, pp. 807–818.
- Thomson, J., Brown, L., Nixon, S., Cook, G.T., MacKenzie, A.B., 2000. Bioturbation and Holocene sediment accumulation fluxes in the north-east Atlantic Ocean (Benthic Boundary Layer experiment sites). *Mar. Geol.* 169, 21–39.
- Thomson, J., Mackenzie, A.B., Cook, G.T., Harkness, D.D., 1993. Application of Radionuclide Studies to the BOFS Programme in NERC Biogeochemical Ocean Flux Study Community Research Project 1987–1993. Final Reports on Special Topic Awards, vol. 2. Natural Environment Research Council, UK.
- Véron, A., Church, T., Patterson, C., Flegal, A., 1994. Use of stable lead isotopes to characterise the sources of anthropogenic lead in North Atlantic surface waters. *Geochim. Cosmochim. Acta* 58, 3199–3206.
- Véron, A., Church, T., 1997. Use of stable lead isotopes and trace metals to characterize air mass sources into eastern North Atlantic. *J. Geophys. Res.* 102, 28049–28058.
- Véron, A., Church, T., Rivera-Duarte, I., Flegal, A., 1999. Stable lead isotopic ratios trace thermohaline circulation in subarctic North Atlantic. *Deep-Sea Res. Part II* 46, 919–935.
- Vogt, R., Jung, W.Y., 2004. The Terceira Rift as hyperslow, hotspot dominated oblique spreading axis: a comparison with other slow spreading plate boundaries. *Earth Planet. Sci. Lett.* 218, 77–90.
- Wessel, P., Sandwell, D.T., Kim, S.S., 2010. The global seamount census. *Oceanography* 23, 24–33.
- Wildeman, T.R., Haskin, L.A., 1965. Rare-earth elements in ocean sediments. *J. Geophys. Res.* 70, 2905–2910.
- Zhou, Y., Bohor, B.F., Ren, Y., 2000. Trace element geochemistry of altered volcanic ash layers (tonsteins) in Late Permian coal-bearing formations of eastern Yunnan and western Guizhou Provinces, China. *Int. J. Coal Geol.* 44, 305–324.